Astronomy & Astrophysics

Radiative transition rates and collision strengths for Si II[⋆]

M. A. Bautista[1], P. Quinet[2,3], P. Palmeri[2], N. R. Badnell[4], J. Dunn[5], and N. Arav[5]

1 Department of Physics, Western Michigan University, Kalamazoo, MI 49008-5222, USA
   e-mail: manuel.bautista@wmich.edu
2 Astrophysique et Spectroscopie, Université de Mons-Hainaut, 7000 Mons, Belgium
3 IPNAS, B15 Sart Tilman, Université de Liège, 4000 Liège, Belgium
4 Department of Physics, University of Strathclyde, Glasgow G4 0NG, UK
5 Department of Physics, Virginia Polytechnic Institute and State University, Blacksburg, VA 24061, USA

ABSTRACT

Aims. This work reports on radiative transition rates and electron impact excitation collision strengths for levels of the $3s^23p$, $3s3p^2$, $3s^24s$, and $3s^23d$ configurations of Si II.
Methods. The radiative data were computed using the Thomas-Fermi-Dirac-Amaldi central potential, but with the modifications introduced by Bautista (2008) that account for the effects of electron-electron interactions. We also introduce new schemes for the optimization of the variational parameters of the potential. Additional calculations were carried out with the Relativistic Hartree-Fock and the multiconfiguration Dirac-Fock methods. Collision strengths in LS-coupling were calculated in the close coupling approximation with the *R*-matrix method. Then, fine structure collision strengths were obtained by means of the intermediate-coupling frame transformation (ICFT) method which accounts for spin-orbit coupling effects.
Results. We present extensive comparisons between the results of different approximations and with the most recent calculations and experiments available in the literature. From these comparisons we derive a recommended set of gf-values and radiative transition rates with their corresponding estimated uncertainties. We also study the effects of different approximations in the representation of the target ion on the electron-impact collision strengths. Our most accurate set of collision strengths were integrated over a Maxwellian distribution of electron energies and the resulting effective collision strengths are given for a wide range of temperatures. Our results present significant differences from recent calculations with the B-spline non-orthogonal *R*-matrix method. We discuss the sources of the differences.

Key words. atomic data – atomic processes – line: formation – quasars: absorption lines – Sun: abundances – ISM: atoms

1. Introduction

Singly ionized silicon (Si II) is prominent in ultra-violet (UV) and optical spectra of various astrophysical plasmas. In terms of absorption spectra, in the spectral range longward of 912 Å Si II has 8 absorption line complexes connected to the ground term $3s^23p$ $^2P^\circ$. In photoionized plasmas with electron temperatures (T_e) of the order of 10^4 K and electron densities (n_e) ≤ 10^4 cm^{-3} the relative optical depths of troughs from the two ground state levels depend on n_e. Hence, this dependence can be used as diagnostic of n_e (e.g. Dunn et al. 2009). On this regard, the lines centered at 1814 Å ($3s^23p$ $^2P^\circ$ – $3s3p^2$ ^2D) are particularly convenient because of their unusually small oscillator strengths, such that these, among all other Si II lines, are the most likely to be in the linear part of the curve of growth and their column densities can be accurately measured. Unfortunately, though, the determination of accurate and reliable oscillator strengths for these transitions is particularly difficult

and has been the subject of much theoretical and experimental efforts.

Si II is also prominent in emission spectra of various kinds of objects. In the upper chromosphere and lower transition region in the Sun and late-type stars line ratios among the Si II 1814 Å multiplet and the intercombination ($3s^23p$ $^2P^\circ$ – $3s3p^2$ ^4P) multiplet near 2335 Å are potentially useful density diagnostics. However, until recently the best electron impact collision strengths of Dufton & Kingston (1991) led to predicted line ratios that disagreed with observations (Judge et al. 1991). Similarly, theoretical models of emission spectra of Broad Line Regions of Active Galactic Nuclei fail to reproduce the observed intensities by factors of a few; a problem that was named by Baldwin et al. (1996) the "Si II disaster".

Despite considerable theoretical work on oscillator strengths there is still considerable spread in the results, particularly for those transitions of most astronomical interest, such as those of the 1814 Å complex. This is because the upper ^2D term of these transitions is made of a mixture of the $3s3p^2$ and $3s^23d$ configurations, which produce strong cancellation in the oscillator strengths and makes the f-values very difficult to compute. Also for these transitions, there has been much spread in experimental gf-values. Measurements based on the electron beam phase shift method (Savage & Lawrence 1966; Curtis & Smith 1974)

---

could be inaccurate for very long lifetimes. Absolute emission measurements on an arc (Hofmann 1969) are often uncertain owing to the difficult control and calibration of the instrument. Determinations based in comparisons of equivalent widths of the weak 1810 Å lines to stronger lines in astronomical spectra (Shull et al. 1981; Van Buren 1986) are unreliable due to blends and saturation of the stronger lines (Jenkins 1986). The latest, and probably most accurate determination of gf-values for these lines was done with the time-resolved laser-induced fluorescence technique Bergeson & Lawler (1993).

The oscillator strengths for the intercombination transitions ($3s^23p\ ^2P^\circ - 3s3p^2\ ^4P$) have also been subject of controversy. These transitions arise due to spin-orbit mixing of the metastable term $3s3p^2\ ^4P$ with the ^2S, ^2P, and ^2D terms. The difficulty then comes from the fact that the gf-values are sensitive to core-valence and core-core correlations, in addition to the valence-shell effects. The results of some of the most recent calculations (Froese Fischer et al. 2006) differ from experimentally measured transition probabilities (Calamai et al. 1993) by $\sim$30%.

But beyond providing accurate oscillator strengths by tailoring atomic structure representations on each type of transition of interest, it is important to try constructing a single representation that yields reasonably accurate energies and oscillator strengths for all levels and transitions considered simultaneously. This is because various practical applications will require such a general atomic representation for subsequent scattering calculations (e.g. electron impact excitation, photoionization, and recombination). One of the most widely used methods for this purpose is based on the Thomas-Fermi-Dirac-Amaldi (TFDA) central potential to generate optimized one-electron orbitals, which represent the atomic structure through configuration interaction (CI) expansions and can also be used for close-coupling representations of the scattering problem. Recently, Bautista (2008) introduced a correction to the TFDA potential that accounts for the effects of electron-electron interactions on the radial wavefunction and yield a considerably improved representation of the system. It is thus interesting to apply this new approach to get the best possible representation of the important Si II system.

In the present paper, to complement and expand the work with the TFDA potential we also compare with the results of the Hartree-Fock Relativistic (HFR), and the multi-configuration Dirac-Fock (MCDF) methods. This general multiplatform approach was successfully employed in our previous studies of the K-shell spectra of Fe, O, Ne, Mg, Si, S, Ar, Ca, and Ni (e.g. Bautista et al. 2003; García et al. 2005; Palmeri et al. 2003a,b, 2008a,b). This has the advantage that allows for consistency checks and inter-comparison. It also helps to reveal which physical processes are important for any given transition, since these different platforms employ different approaches to, for example, relativistic effects and orthogonal vs. non-orthogonal orbitals.

The present paper is organized as follows: in the next section we describe the calculations of oscillator strengths and transition rates. In Sect. 3 we present the calculations of collision strengths, including some new techniques specifically designed for the present problem. Our discussion of the results and conclusions are presented in Sect. 4.

2. Radiative calculations

The Breit-Pauli Hamiltonian for an N-electron system is given by

$$H_{\rm bp} = H_{\rm nr} + H_{\rm 1b} + H_{\rm 2b} \tag{1}$$

where $H_{\rm nr}$ is the usual non-relativistic Hamiltonian, and $H_{\rm 1b}$ and $H_{\rm 2b}$ are the one-body and two-body operators. The one-body relativistic operators

$$H_{\rm 1b} = \sum_{n=1}^{N} f_n({\rm mass}) + f_n({\rm d}) + f_n({\rm so}) \tag{2}$$

represent the spin-orbit interaction, $f_n({\rm so})$, and the non-fine structure mass-variation, $f_n({\rm mass})$, and one-body Darwin, $f_n({\rm d})$, corrections. The two-body corrections

$$H_{\rm 2b} = \sum_{n>m} g_{nm}({\rm so}) + g_{nm}({\rm ss}) + g_{nm}({\rm css}) + g_{nm}({\rm d}) + g_{nm}({\rm oo}), \tag{3}$$

usually referred to as the Breit interaction, include, on the one hand, the fine structure terms $g_{nm}({\rm so})$ (spin-other-orbit and mutual spin-orbit) and $g_{nm}({\rm ss})$ (spin-spin); and on the other, the non-fine structure terms: $g_{nm}({\rm css})$ (spin-spin contact), $g_{nm}({\rm d})$ (Darwin) and $g_{nm}({\rm oo})$ (orbit-orbit).

The oscillator strengths (f-values) for dipole allowed transitions have equivalent forms in length and velocity gauges as

$$f_{jk} \equiv \frac{2m(E_k - E_j)}{\hbar^2}|\langle|j|\mathbf{x}|k\rangle|^2 = \frac{i2m}{\hbar^2}|\langle|j|\mathbf{v}|k\rangle|^2. \tag{4}$$

The radiative rates (A-values) for electric dipole and quadrupole transitions are respectively given in units of s^{-1} by the expressions

$$A_{\rm E1}(k, i) = 2.6774 \times 10^9 (E_k - E_i)^3 \frac{1}{g_k} S_{\rm E1}(k, i) \tag{5}$$

$$A_{\rm E2}(k, i) = 2.6733 \times 10^3 (E_k - E_i)^5 \frac{1}{g_k} S_{\rm E2}(k, i) \tag{6}$$

where $S(k, i)$ is the line strength, g_k is the statistical weight of the upper level, and energies are in Rydberg units and lengths in Bohr radii.

Similarly for magnetic dipole and quadrupole transitions, the A-values are respectively given by

$$A_{\rm M1}(k, i) = 3.5644 \times 10^4 (E_k - E_i)^3 \frac{1}{g_k} S_{\rm M1}(k, i) \tag{7}$$

$$A_{\rm M2}(k, i) = 2.3727 \times 10^{-2} (E_k - E_i)^5 \frac{1}{g_k} S_{\rm M2}(k, i). \tag{8}$$

Due to the strong magnetic interactions in this ion, the magnetic dipole line strength is assumed to take the form

$$S_{\rm M1}(k, i) = |\langle|k|\mathbf{P}|i\rangle|^2 \tag{9}$$

where

$$\mathbf{P} = \mathbf{P^0} + \mathbf{P^1} = \sum_{n=1}^{N}\{\mathbf{l}(n) + \sigma(n)\} + \mathbf{P}^{\rm rc}. \tag{10}$$

$\mathbf{P}^0$ is the usual low-order M1 operator while $\mathbf{P}^{\rm rc}$ includes the relativistic corrections established by Drake (1971).

In the present work we employ three different computational packages to study the properties of the strongly correlated configurations $3s^23p$, $3s3p^2$, $3s^23d$, and $3s^24s$ of Si II.

AUTOSTRUCTURE

AUTOSTRUCTURE, an extension by Badnell (1986, 1997) of the atomic structure program SUPERSTRUCTURE (Eissner et al. 1974), computes fine-structure level energies, radiative and Auger rates in a Breit-Pauli relativistic framework. Single electron orbitals, $P_{nl}(r)$, are constructed by diagonalizing the non-relativistic Hamiltonian, H_{nr}, within a statistical Thomas-Fermi-Dirac-Amaldi (TFDA) model potential $V(\lambda_{nl})$ (Eissner & Nussbaumer 1969). The λ_{nl} scaling parameters are optimized variationally by minimizing a weighted sum of the LS term energies. LS terms are represented by configuration-interaction (CI) wavefunctions of the type:

$$\Psi(LS) = \sum_i c_i \phi_i. \qquad (11)$$

Bautista (2008) introduced a modification to the TFDA model potential that accounts in part for the effects of electron-electron correlations on the radial wavefunctions by means of additional higher order terms in the potential whose strength is controlled by variational parameters. We will refer to this potential as c-TFDA. This formalism also proposed a new optimization technique of the variational parameters by minimizing the difference between predicted, including spin-orbit coupling and relativistic effects, and experimental term averaged energies. The numerical functional used for this optimization was:

$$F = \sum_i \frac{|E_i^{\text{obs}} - E_i^{\text{theo}}| + \epsilon}{E_i^{\text{obs}}} \qquad (12)$$

with E_i^{obs} and E_i^{theo} the observed and theoretical energies respectively of term i and

$$\epsilon = \max\{0, (E_{\text{core}} - E_{\text{core}}^0)\}.$$

This last term acts as a penalty to the functional whenever the new core energy exceeds that found from the standard TFDA minimization. This numerical functional was modified again for the present work as shown in Sect. 2.2.

HFR

In the Hartree-Fock Relativistic code (HFR) by Cowan (1981), a set of orbitals are obtained for each electronic configuration by solving the Hartree-Fock equations for the spherically averaged atom. The equations are the result of the application of the variational principle to the configuration average energy. Relativistic corrections are also included in this set of equations, i.e. the Blume-Watson spin-orbit, mass-variation and one-body Darwin terms. The Blume-Watson spin-orbit term comprises the part of the Breit interaction that can be reduced to a one-body operator.

The multi-configuration Hamiltonian matrix is constructed and diagonalized in the $LSJ\pi$ representation within the framework of the Slater-Condon theory. Each matrix element is a sum of products of Racah angular coefficients and radial integrals (Slater and spin-orbit integrals), i.e.

$$\langle a|H|b \rangle = \sum_i c_i^{a,b} I_i^{a,b}. \qquad (13)$$

The radial parameters, $I_i^{a,b}$, can be adjusted to fit the available experimental energy levels in a least-squares approach. The eigenvalues and the eigenstates obtained in this way (ab initio or semi-empirical) are used to compute the wavelength and oscillator strength for each possible transition.
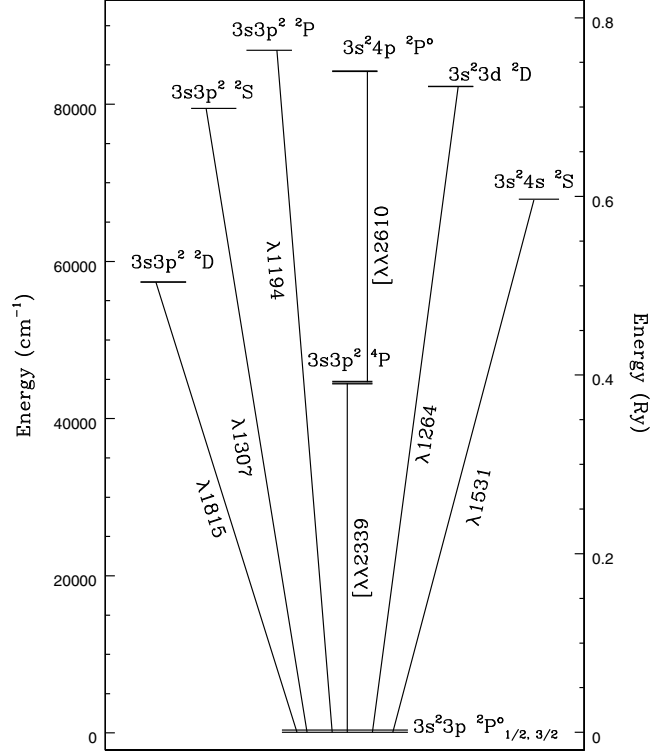
Fig. 1. Partial Grotrian diagram of Si ɪɪ showing the 22 lowest Levels in 8 LS terms and the dipole and intercombination line multiplets observable in the UV spectral region.

MCDF

The multi-configuration Dirac-Fock (MCDF) method considers the Dirac Hamiltonian for a N-electron atomic system given in au by:

$$H_D \equiv \sum_{i=1}^{N} \left[c\alpha_i \times \mathbf{p}_i - (\beta_i - 1)c^2 - \frac{Z}{r_i} \right] + \sum_{i \neq j}^{N} \frac{1}{r_{ij}}, \qquad (14)$$

where c is the speed of light and α and β are the Dirac matrices. The atomic state function (ASF) is given as an expansion over jj-coupled configuration state functions (CSFs), which in turn are constructed from Slater determinants built on four-component Dirac orbitals. The MCDF method is implemented in the computer package GRASP2K, described by Jöönsson et al. (2007).

2.1. Energy levels and radiative rates

Our calculations concentrate on the 15 lowest levels, of the Si ɪɪ system. This is 8 LS terms from configurations $3s^23p$, $3s3p^2$, $3s^24s$, $3s^23d$, and $3s^24p$. A Grotrian diagram of the ions is presented in Fig. 1 which shows the levels and the UV optical and intercombination transitions of interest.

2.1.1. Calculations with HFR

In the physical model adopted in HFR calculations, we suppose that the Si$^+$ ion can be represented by three valence electrons surrounding a Ne-like Si^{4+} ionic core with ten electrons occupying the $1s^22s^22p^6$ closed subshells. The intravalence correlation is then considered by the explicit introduction, in the

model, of the 52 following configurations: 3s23p + 3s24p + 3s25p + 3s^{2}4f + 3s^{2}5f + 3s3p3d + 3s3p4d + 3s3p5d + 3s3p4s + 3s3p5s + 3s3d4p + 3s3d5p + 3p^{2}4p + 3p^{2}5p + 3p^{2}4f + 3p^{2}5f + 3d^{2}4p + 3d^{2}5p + 3d^{2}4f + 3d^{2}5f + 3p^3 (odd parity) and 3s3p^2 + 3s^{2}4s + 3s^{2}5s + 3s^{2}3d + 3s^{2}4d + 3s^{2}5d + 3s3p4p + 3s3p5p + 3s3p4f + 3s3p5f + 3s3d^2 + 3s4s^2 + 3s4p^2 + 3s4d2 + 3s4s5s + 3s3d4s + 3s3d5s + 3s3d4d + 3s3d5d + 3p^{2}3d + 3p^{2}4d + 3p^{2}5d + 3p^{2}4s + 3p^{2}5s + 3p3d4p + 3p4s4p + 3d^{2}4s + 3d^{2}5s + 3d^{2}4d + 3d^{2}5d +3d^3 (even parity). Core-valence correlation is then considered by including a core-polarization (CPOL) potential and a correction to the dipole operator as described in many previous papers (see e.g. Quinet et al. 1999, 2002). These corrections are used with a value of the dipole polarizability equal to 0.16 a_0^3, as computed by Johnson et al. (1983) for Si V, and a cut-off radius equal to 0.53 a_0 which corresponds to the HFR expectation value of $\langle r \rangle$ for the outermost core orbital, i.e. 2p. This method is then combined with a well-established least-squares optimization of the radial parameters in order to minimize the discrepancies between the Hamiltonian eigenvalues and the available experimental energy levels for the 3s23p, 3s^{2}4p, 3s3p^2, 3s^{2}4s, 3s^{2}5s, 3s^{2}3d, 3s^{2}4d, 3s^{2}5d and 3s3p4p configurations.

2.1.2. Calculations with MCDF

Here, we carried out two MCDF calculations. The first one, hereafter referred to as MCDF1, was focused on our radiative parameters for the intercombination transitions 3s^{2}3p ^{2}P° − 3s3p^2 ^{4}P, and the second one, hereafter referred to as MCDF2, on those of the allowed transitions 3s^{2}3p ^{2}P° − 3s3p^2 ^{2}D.

In MCDF1, CI expansions are built including the valence-valence correlation through single and double excitations from 3s^{2}3p $J = 1/2, 3/2 + 3s3p^2$ $J = 1/2, 3/2, 5/2$ extending the orbital active set up to 5g in 4 steps. The final number of CSFs generated was 2127. For 3 of the steps, we selected an "extended optimal level", EOL, optimization option (Dyall et al. 1989; Parpia et al. 1996) on the lowest 5 levels using the same weight for the 5 ASFs. In the first step, no excitation was allowed, the active set was limited up to 3p, and all the core and valence orbitals were variational. The second step consisted in extending the expansion through single and double excitations increasing the active set up to 3d. Here, only the 3d orbital was variational, while freezing all the others to their values of the preceding optimization step. In the third step, the expansions were further extended increasing the active set up to 4f. All $n = 4$ orbitals were optimized while freezing all others in a similar procedure as in the second step. In the final optimization step, only the $n = 5$ were variational freezing all the other orbitals to their preceding step values.

In MCDF2, we used the same procedure as in MCDF1 except that the excitations were from 3s^{2}3p $J = 1/2, 3/2 + 3s3p^2$ $J = 3/2, 5/2$ and the EOL option was selected on the first, second, fifth and sixth levels. Here the final number of CSFs used in the MCDF expansions was 1832.

2.1.3. Calculations with AUTOSTRUCTURE

We performed calculations with various different configurations expansions, starting with models similar to those of previously published work and then evolving to more sophisticated techniques and larger configuration expansions.

Table 1 presents the configurations included in 7 basic expansions studied. The various configuration expansions (CEs) are named CE1, CE2, ..., CE6 and are tabulated in such a way

Table 1. Configurations included in various expansions used for Si II.

CE1	2s^{2}2p^{6}3s^{2}3p, 2s^{2}2p^{6}3s3p^2, 2s^{2}2p^{6}3s3p3d, 2s^{2}2p^{6}3s3d^2, 2s^{2}2p^{6}3p^3, 2s^{2}2p^{6}3p^{2}3d, 2s^{2}2p^{6}3p3d^2, 2s^{2}2p^{6}3d^3, 2s^{2}2p^{6}3s^{2}3d, 2s^{2}2p^{6}3s^{2}4s, 2s^{2}2p^{6}3s^{2}4p, 2s^{2}2p^{6}3s^{2}4d, 2s^{2}2p^{6}3s^{2}5s, 2s^{2}2p^{6}3s^{2}5p, 2s^{2}2p^{6}3s^{2}5d, 2s^{2}2p^{6}3s3p4s, 2s^{2}2p^{6}3s3p4p, 2s^{2}2p^{6}3s3d4p, 2s^{2}2p^{6}3s3d4d, 2s^{2}2p^{6}3s4p^2, 2s^{2}2p^{6}3s4s5s, 2s^{2}2p^{6}3p^{2}4s, 2s^{2}2p^{6}3p3d4p, 2s^{2}2p^{6}3d^{2}4s
CE2	2s^{2}2p^{6}3s^{2}4f, 2s^{2}2p^{6}3s^{2}5f
CE3	2s^{2}2p^{5}3s^{2}3p^2, 2s^{2}2p^{5}3s^{2}3p3d, 2s^{2}2p^{5}3s^{2}3p4s
CE4	2s^{2}3p^{4}3s^{2}3p^3, 2s^{2}2p^{4}3s^{2}3p^{2}3d, 2s^{2}2p^{4}3s^{2}3p^{2}4s
CE5	2s2p^{6}3s^{2}3p^2, 2s2p^{6}3s^{2}3p3d, 2s2p^{6}3s^{2}3p4s
CE6	2s^{2}2p^{5}3s^{2}3p4p, 2s^{2}2p^{5}3s^{2}3p4d, 2s^{2}2p^{4}3s^{2}3p^{2}4p, 2s^{2}2p^{4}3s^{2}3p^{2}4d, 2s^{2}2p^{3}3s^{2}3p^4, 2s^{2}2p^{3}3s^{2}3p^{3}3d, 2s^{2}2p^{3}3s^{2}3p^{3}4s, 2s^{2}2p^{3}3s^{2}3p^{3}4p, 2s^{2}2p^{3}3s^{2}3p^{3}4d

that each CE includes the configurations of all previous CEs. In other words, CE1 includes the 24 configurations listed at the top of Table 1, CE2 includes all 24 configurations from CE1 plus 2s^{2}2p^{6}3s^{2}4f, CE3 includes the 25 configuration from CE1 and CE2 plus 3 more, and CE6 includes all 48 configurations in the table.

The rational for these configurations and the progression of various calculations carried is as follows:

– **AST1**: this calculation uses the expansion CE1 that keeps the 2s and 2p shells closed and promotes the three remaining electrons among orbitals with principal quantum number $n = 3-5$ and orbital angular momentum $l = 0-2$. The TFDA potential was used and the orbitals were optimized in the standard AUTOSTRUCTURE procedure minimizing the energies of the lowest 8 LS terms. Fine structure coupling and relativistic corrections are introduced as perturbations after optimizing the orbitals. From this calculation the core energy of the system is −578.40 Ry. Table 1 compares the calculated energies relative to the ground level with experimental values from NIST (2008). The results are rather unsatisfactory with energy differences scattered between −19% and 35%. Even more troublesome are the gf-values that result from this calculation, particularly those for the 1814 Å multiplet, which are considerably overestimated with respect to the experimental determination of Bergeson & Lawler (1993) (see Fig. 2). This is because it is difficult to represent 3s^{2}3p and 3s3p^2 states simultaneously with orthogonal orbitals, owing to polarization and orbital relaxation effects.

– **AST2**: for this calculation we use the same expansion CE1 as in AST1 but with the use of the c-TFDA potential of Bautista (2008) optimized against the experimental term energies using the functional of Eq. (12). This gave a core energy of −578.34 Ry, which is slightly higher than in AST1. Yet, the calculated energies here agree much better with experiment than from AST1, with most terms within 5% of experiment with the exception of the two excited levels 3s^{2}3p ^{2}P°$_{3/2}$, from the ground multiplet, and 3s3p^2 ^{4}P$_j$. Together with the changes in calculated energies there are also significant changes in the predicted gf-values for the 1814 Å and 1531 Å multiplets, as illustrated in Fig. 2.

– **AST3**: this calculation is just like AST2, but we now add the configurations 3s^{2}4f and 3s^{2}5f (i.e. CE2). We find that the f orbitals have an important effect on increasing the
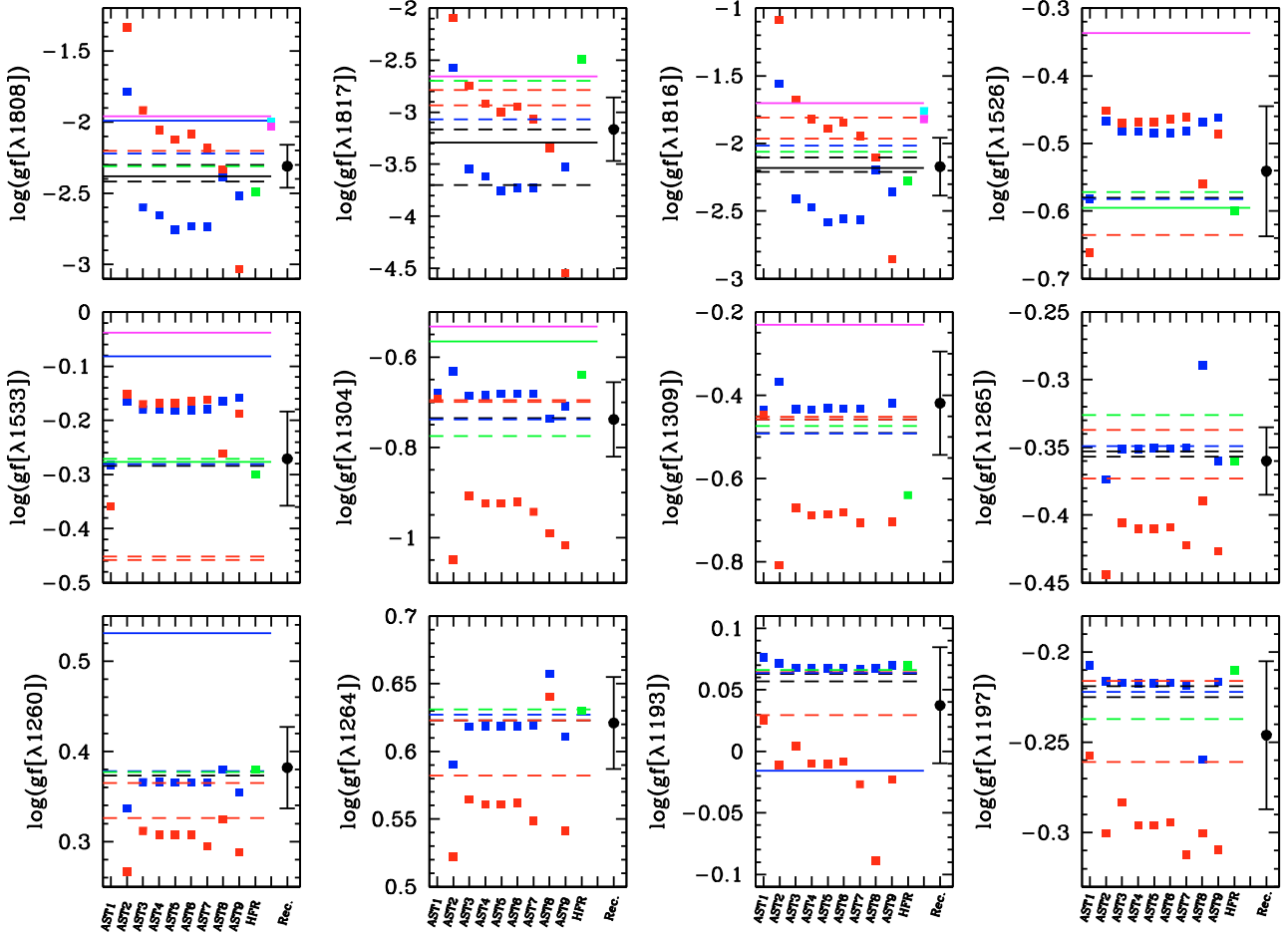
Fig. 2. Evolution of the gf-values for transitions in Si II from our different calculations AST1, ..., AST9 and comparison with previous determinations. The square points depict our results in the length gauge (blue) and velocity gauge (red). The solid horizontal lines depict experimental determinations by Shull et al. (1981) (magenta), Van Buren (1986) (blue), Schectman et al. (1988) (green), Bergeson & Lawler (1993) (black). The dashed lines depict theoretical results of Froese Fischer et al. (2006), (blue), Tayal (2007) (red), Nahar (1988) (green).

polarizability of configurations that include d orbitals, such as the 3s3d^2, and 3p^{2}3d. Thus, by including nf configurations in the expansion we find different optimization for the core. When including these nf orbitals one has to include enough nd configurations in order to reach convergence in the solution. But, various configurations such as 3d, 3d2, 4d, and 5d are already included since CE1. In the course of the calculations we checked on the contributions of 5d and 5f and they were found to be small. Thus, we believe that the calculation is nearly converged. In this calculation the core energy improves to −578.38 Ry and the agreement between calculated and experimental energies with respect to the ground level also improves a little. Despite the relatively minor changes in the calculated energies between this calculation and the previous one there are large changes in the gf-values for the 1814 Å and 1264 Å multiplets, with a drop of ~0.8 dex for the former and a rise of ~0.9 dex for the latter.

– **AST4**, **AST5**, **AST6**, and **AST7**: for these calculations we progressively add new configurations by opening the 2s and 2p orbitals, with one 2p electron promotions in AST4 (CE3), two 2p electron promotions in AST5 (CE4), one 1s electron promotions in AST6 (CE5) and three 2p electron promotions in AST7 (CE6). By this point the computational time in optimizing all orbitals of the potential has become exceedingly

long, going from a few minutes in the AST1 calculation to several hours in the AST7 calculation. For this reason, and with the purpose to see the effects of increasing CI we did not optimize again the orbitals for these calculation, but instead chose the same scaling parameters as in AST3. Despite the large increase in CI in these computations we find no significant change in either the calculated energies, see Table 2. The calculated core energies also remain constant at −578.38 Ry for **AST4**, **AST5**, and **AST6** and −578.39 Ry for **AST7**. The computed f-values are also unaltered by CI, except for those of the 1814 Å multiplet which seem to converge asymptotically. Nonetheless, for this and most of the other transitions the difference between length and velocity gauges of the f-values is uncomfortably large. It is clear now that increasing the amount of CI in the calculations beyond that of the AST7 calculation will not improve the quality of the results. Instead, we need to turn our attention towards the optimization of the orbitals.

– **AST8**: for this calculation we decided to return to the simplest expansion CE1, but try a different optimization technique. Because the f-values for the 1814 Å multiplet is so sensitive to cancellation in the mixing of the 3s3p^2 ^{2}D and 3s^{2}3d ^{2}D states it is crucial to reproduce the experimental energies of the levels as accurately as possible. Thus, we

Table 2. Comparison of level energies (Ry) for Si II.

Level	Exp.	AST1	AST2	AST3	AST4	AST5	AST6	AST7	AST8	AST9
						Difference from experiment(%)				
$3s^2 3p\ ^2P^\circ_{1/2}$	0.0	0.0	0.0	0.0	0.0	0.0	0.0	0.0	0.0	0.0
$3s^2 3p\ ^2P^\circ_{3/2}$	0.002618	−18.8	−17.8	−14.8	−15.0	−15.0	−15.0	−15.1	0.19	−0.12
$3s3p^2\ ^4P_{1/2}$	0.390244	−7.86	−17.4	−11.3	−11.3	−10.9	−10.9	−10.6	−7.06	−7.62
$3s3p^2\ ^4P_{3/2}$	0.391231	−7.90	−17.4	−11.4	−11.3	−10.9	−10.9	−10.6	−7.01	−7.57
$3s3p^2\ ^4P_{5/2}$	0.392828	−7.96	−17.4	−11.4	−11.3	−10.9	−10.9	−10.6	−6.92	−7.48
$3s3p^2\ ^2D_{3/2}$	0.504016	14.5	2.42	1.03	1.00	1.18	1.18	1.42	−0.01	−0.25
$3s3p^2\ ^2D_{5/2}$	0.504160	14.4	2.40	1.01	0.98	1.15	1.16	1.39	−0.02	−0.27
$3s^2 4s\ ^2S_{1/2}$	0.596884	−0.53	3.31	−0.39	−0.49	−0.59	−0.54	−0.32	15.3	−4.64
$3s3p^2\ ^2S_{1/2}$	0.698626	0.69	1.64	3.23	3.25	3.46	3.46	3.60	2.73	1.78
$3s^2 3d\ ^2D_{3/2}$	0.722986	35.3	−2.37	1.19	1.13	1.14	1.17	1.29	11.1	10.3
$3s^2 3d\ ^2D_{5/2}$	0.723136	35.2	−2.39	1.17	1.12	1.12	1.16	1.28	11.1	10.3
$3s^2 4p\ ^2P^\circ_{1/2}$	0.739870	22.0	3.40	6.77	6.83	7.03	7.07	6.81	13.9	13.7
$3s^2 4p\ ^2P^\circ_{3/2}$	0.740416	22.3	3.41	6.82	6.87	7.08	7.12	6.86	14.0	13.9
$3s3p^2\ ^2P_{1/2}$	0.763660	0.75	5.74	5.52	5.49	5.68	5.71	5.74	4.20	5.01
$3s3p^2\ ^2P_{1/2}$	0.765503	0.69	5.68	5.47	5.44	5.64	5.66	5.70	4.21	5.04

modified the AUTOSTRUCTURE code use an optimization functional of the form

$$F = \sum_i \frac{w_i (E_i^{\text{obs}} - E_i^{\text{theo}})^2 +}{(E_i^{\text{obs}})^2} + \epsilon, \qquad (15)$$

where the sum goes over fine structure energy levels and w_i is a user defined weight on different levels. For our calculation we ran this sum for the lowest 15 levels of the Si II system and we weighted the $3s^2 3p\ ^2P^\circ_{3/2}$ and $3s3p^2\ ^2D_J$ levels 5 times as much as the rest. This kind of optimization provides much better energies for all levels and nearly exact energies for the $3s^2 3p\ ^2P^\circ_{3/2}$ and $3s3p^2\ ^2D_J$ levels (within 0.2% of experiment). This optimization also provides a lower core energy than from previous calculations (−578.42 Ry). Nevertheless, this optimization does not reduce the difference between length and velocity forms of the f-values.

An alternative optimization functional that is already available in AUTOSTRUCTURE is based on the differences between length and velocity f-values. This, however, does not work because it leaves the level energies to change way off from experiment.

Then, we define a combined functional of the form

$$F = \sum_i \frac{w_i (E_i^{\text{obs}} - E_i^{\text{theo}})^2 + \epsilon}{(E_i^{\text{obs}})^2}$$
$$+ \sum_i \sum_j \frac{w_i (gf_{ij}^{\text{l}} - gf_{ij}^{\text{v}})^2}{(gf_{ij}^{\text{l}} + gf_{ij}^{\text{v}})^2}, \qquad (16)$$

where gf_{ij}^{l} and gf_{ij}^{v} are the length and velocity forms of the gf-value for the transition $i \rightarrow j$. An optimization of this kind heavily weighted on the gf-values for the 1260 Å multiplet yields length and velocity values in very close agreement with each other. These results also agree very well with the experimental determination of Bergeson & Lawler (1993). Unfortunately, the obtained gf-values for transitions involving higher terms seem to deteriorate. This is to be expected, as the small expansion used here misses important core-valence and core-core correlations.

– **AST9**: for this last calculation we use the largest expansion CE6 and optimize the orbitals as in **AST8**. For a model expansion of this size numerical optimization becomes challenging, and the code took 4 days to do so. The resulting energies are slightly better than in the previous calculation, and the core energy is predicted at −572.41 Ry. It is found that the f-values in the length gauge for the 1814 Å multiplet remain in good agreement with the experiment of Bergeson & Lawler (1993) although the velocity f-value departed somewhat. Interestingly, for these transitions the present velocity f-value is lower than the length f-value, contrary to what was seen in previous calculations. The present difference between the two forms of the f-value probably owes to the need of finer optimization of the orbitals, which became computationally prohibitive for the large CI expansion used here. Another interesting set of f-values are those for the 1260 Å multiplet, which in the present calculation result somewhat higher and with greater difference between length and velocity than from previous calculations. The present result seems to favor the experimental determination of Schectman et al. (1988), while the results of previous calculations seemed very stable and in good agreement with Froese Fischer et al. (2006) and Tayal (2007).

At this point is worth pointing out the detailed study of Dufton et al. (1992) on the LS f-value for the 1814 Å transition. They found that in dealing with the cancelation effects from contributions from the $3s3p^2\ ^2D$ and $3s^2 3d\ ^2D$ states one must pay attention to the calculated energy difference between these states. In this sense we notice that our prefer calculation AST8 and AST9 yield energy separations for the $3s3p^2\ ^2D$ and $3s^2 3d\ ^2D$ states that differ by ~10–11% from experiment, in contrast with calculations AST3 through AST7 that reproduce these energy separation significantly better. However, getting exact energies is neither sufficient nor guarantee of resulting accurate gf-vaues. Inspection of Table 1 of Dufton et al. (1992) shows that essentially the same gf-value can obtained when the energy difference with respect to experiment was less than 2% and nearly 11%. By contrast, calculations that predicted energies differing from experiment by 5 and 7% got gf-values that were off by roughly a factor of 3. Moreover, we are mostly concerned with the fine structure gf-values and for that we also need accurate energies for the J resolved levels of the $3s^2 3p\ ^2P$ and $3s3p^2\ ^2D$ terms and these are best reproduced by the AST8 and AST9 calculations, as opposed to the AST7 calculation that underestimates the energy of the $3s^2 3p\ ^2P_{3/2}$ level by 15%.
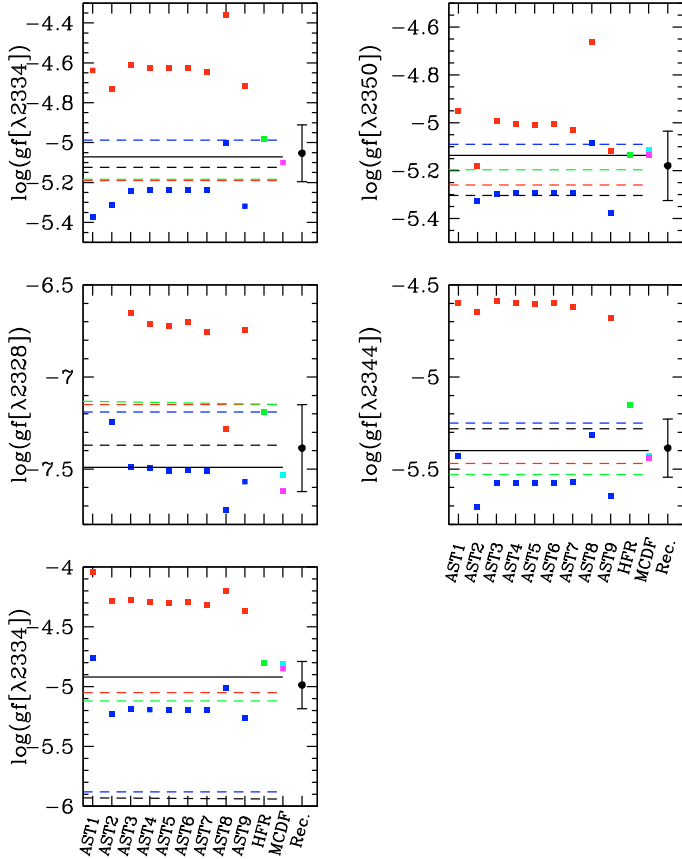
Fig. 3. Evolution of the gf-values for intercombination transition in Si II from our different calculations AST1, ..., AST9 and comparison with experimental values of Calamai et al. (1993). The square points depict our results in the length gauge (blue) and velocity gauge (red). The experimental vales are given by the horizontal solid line, with quoted errors given by dashed lines.

On the other hand, it is also known that in computing gf-values one may not rely only on the agreement between length and velocity values, because such an criterium can be misleading if the model potential is oversimplified. Nonetheless, we believe that the agreement between length and velocity results in our calculations AST8 and, particularly AST9 is very significant. AST9 uses the largest CI expansion that we could handle, which the inner core orbitals to account for polarization. In addition, this calculation uses the c-TFDA potential to account for additional electron-electron correlation. Thus AST9 employs the most complex and complete potential that we can build at this time, then the good agreement between length and velocity seems meaningful.

Now we look at the results for the intercombination transitions $3s^23p\ ^2P^\circ_j - 3s3p^2\ ^4P_{j'}$. These lines, seen in emission in the $2328-2350$ Å spectral range, are very useful density diagnostics in a variety of astronomical sources. Though, computation of accurate transition rates, A-values, for these lines is difficult because the transitions are induced by mixing between the ^4P and even parity doublet states. Hence, the calculated A-values for the intercombination transitions depend critically on the quality of the representation of those even parity doublet states. Figure 3 shows the evolution of the calculated gf-values in length and velocity forms from our calculations together with the results of other authors and the experimental determinations of Calamai et al. (1993). Here we plot our results in the length and

velocity gauges, although none of previous authors present similar comparisons. It is clear, though, that there are considerable discrepancies between the two gauges, being the length form of the gf-values typically in better agreement with experiment. Other authors, like Tayal (2007) do not even quote their results in the velocity gauge. Indeed, the velocity form of the gf-value is typically less stable numerically, since it depends on the first derivative of the radial wavefunction. Thus, we disregard the velocity gf-values for subsequent analysis. The present gf-values from AUTOSTRUCTURE agree within 0.2 dex with experimental determinations of Calamai et al. (1993), and the agreement between MCDF results and experiment is even better, within 0.1 dex. On the other hand, the HFR results seem as accurate as MCDF for some transitions, but significantly discrepant for others. The results of Tayal (2007) and Froese Fischer et al. (2006), using a multiconfiguration Hartree-Fock, are comparable in quality to our HFR results. The results of Dufton & Kingston (1991), based on the multiconfiguration Hartree-Fock method, and Nussbaumer (1977), from the use of the TFDA potential, seem to be of inferior quality.

It seems clear that no one calculation among those performed here and those reported by other authors can provide ultimate accuracy gf-values for all transitions simultaneously. Like with the different calculations, there is significant scatter among the results of various experimental determinations. Thus, in order to provide the most reliable set of gf-values possible we take the statistical average among all theoretical results, i.e. our present results from AST8 and AST9 and those of other authors. In computing the average we discard values that depart by more than 3σ from the average, where σ is the statistical dispersion of the data. Both, length and velocity gf-values, are taken with equal weights in the average. In the case of the recombination transitions and the 1814 Å multiplet we also include in the averages the experimental data from Calamai et al. (1993) and Bergeson & Lawler (1993) respectively with twice as much weight as the theoretical values. It is noted that our calculation AST8 that uses the smaller configuration expansion is very well optimized on the lowest energy terms, for instance the $3s^23p\ ^2P^\circ$ and $3s3p^2\ ^2D$ terms, but it deteriorates rapidly for higher excitation terms. Figure 2 depicts our recommended gf-values for every transition together with the statistical dispersion, which is probably representative of the true uncertainty. In Table 3 we show our results for transitions among the lowest 15 levels of the ion from the AST9, AST9, HFR, and MCDF calculations. The AUTOSTRUCTURE results are given in length and velocity gauges and the MCDF results are given in the corresponding Coulomb and Babushkin gauges. In the last column of the table are our recommended values and estimated uncertainties.

3. Collision strengths

The collision strengths for electron impact excitation are computed with the ICFT Breit-Pauli R-matrix package (BPRM) based on the close-coupling approximation of Burke & Seaton (1971) whereby the wavefunctions for states of an N-electron target and a colliding electron with total angular momentum and parity $J\pi$ are expanded in terms of the target eigenfunctions

$$\Psi^{J\pi} = \mathcal{A} \sum_i \chi_i \frac{F_i(r)}{r} + \sum_j c_j \Phi_j. \tag{17}$$

The functions χ_i are vector coupled products of the target eigenfunctions and the angular components of the incident-electron functions, $F_i(r)$ are the radial part of the projectile electron

Table 3. $\log(gf)$ values for transitions among the 15 lowest levels in Si II.

Lower level	Upper level	λ (Å)	AST8		AST9		HFR	MCDF		Recom.	Error
			$\log(gf)_l$	$\log(gf)_v$	$\log(gf)_l$	$\log(gf)_v$	$\log(gf)$	$\log(gf)_C$	$\log(gf)_B$		
$3s^23p\ ^2P^\circ_{1/2}$	$3s3p^2\ ^4P_{1/2}$	2334.41	−5.00	−4.89	−4.89	−4.55	−4.98	−5.09	−5.10	−5.05	0.14
$3s^23p\ ^2P^\circ_{3/2}$	$3s3p^2\ ^4P_{1/2}$	2350.17	−5.08	−4.66	−4.94	−4.86	−5.13	−5.11	−5.13	−5.18	0.15
$3s^23p\ ^2P^\circ_{1/2}$	$3s3p^2\ ^4P_{3/2}$	2328.52	−7.72	−7.28	−7.49	−8.06	−7.19	−6.53	−6.62	−7.39	0.24
$3s^23p\ ^2P^\circ_{3/2}$	$3s3p^2\ ^4P_{3/2}$	2344.20	−5.32	−4.42	−5.27	−4.59	−5.15	−5.43	−5.44	−5.39	0.16
	$3s3p^2\ ^4P_{5/2}$	2334.20	−5.02	−4.20	−4.94	−4.40	−4.80	−4.81	−4.85	−4.99	0.20
$3s^23p\ ^2P^\circ_{1/2}$	$3s3p^2\ ^2D_{3/2}$	1808.00	−2.39	−2.33	−2.47	−2.90	−2.49	−1.99	−2.03	−2.31	0.16
$3s^23p\ ^2P^\circ_{3/2}$	$3s3p^2\ ^2D_{3/2}$	1817.45	−3.34	−3.34	−3.45	−4.28	−3.45	−2.82	−2.87	−3.14	0.26
	$3s3p^2\ ^2D_{5/2}$	1816.92	−2.20	−2.10	−2.30	−2.72	−2.28			−2.17	0.22
$3s^23p\ ^2P^\circ_{1/2}$	$3s^24s\ ^2S_{1/2}$	1526.72	−0.24	−0.38	−0.46	−0.51	−0.60			−0.54	0.10
$3s^23p\ ^2P^\circ_{3/2}$	$3s^24s\ ^2S_{1/2}$	1533.45	+0.05	−0.11	−0.46	−0.51	−0.30			−0.27	0.09
$3s^23p\ ^2P^\circ_{1/2}$	$3s3p^2\ ^2S_{1/2}$	1304.37	−2.62	−2.07	−0.71	−1.01	−0.64			−0.74	0.09
$3s^23p\ ^2P^\circ_{3/2}$	$3s3p^2\ ^2S_{1/2}$	1309.27	−3.12	−2.83	−0.47	−0.79	−0.41			−0.49	0.09
$3s^23p\ ^2P^\circ_{1/2}$	$3s^23d\ ^2D_{3/2}$	1260.42	+0.39	+0.32	+0.49	+0.40	+0.38			+0.38	0.05
$3s^23p\ ^2P^\circ_{3/2}$	$3s^23d\ ^2D_{3/2}$	1265.02	−0.28	−0.39	−0.58	−0.68	−0.36			−0.40	0.10
	$3s^23d\ ^2D_{5/2}$	1264.73	+0.61	+0.70	+0.61	+0.57	+0.63			+0.62	0.04
$3s^23p\ ^2P^\circ_{1/2}$	$3s3p^2\ ^2P_{1/2}$	1193.28	+0.041	−0.068	+0.060	+0.082	+0.069			+0.037	0.047
$3s^23p\ ^2P^\circ_{3/2}$	$3s3p^2\ ^2P_{1/2}$	1197.39	−0.24	−0.22	−0.34	−0.31	−0.21			−0.25	0.04
$3s^23p\ ^2P^\circ_{1/2}$	$3s3p^2\ ^2P_{3/2}$	1190.42	−0.04	−0.55	−0.68	−0.33	−0.25			−0.29	0.10
$3s^23p\ ^2P^\circ_{3/2}$	$3s3p^2\ ^2P_{3/2}$	1194.50	+0.39	+0.52	+0.39	+0.38	+0.48			+0.28	0.22
$3s3p^2\ ^4P_{1/2}$	$3s^24p\ ^2P^\circ_{1/2}$	2605.62	−6.24	−6.45	−7.39	−6.90	−9.34			−6.56	0.34
$3s3p^2\ ^4P_{1/2}$	$3s^24p\ ^2P^\circ_{3/2}$	2601.56	−6.49	−7.33	−6.54	−6.03	−7.99			−6.50	0.45
$3s3p^2\ ^4P_{3/2}$	$3s^24p\ ^2P^\circ_{1/2}$	2613.00	−5.75	−6.22	−5.95	−6.10	−5.64			−5.88	0.21
$3s3p^2\ ^4P_{3/2}$	$3s^24p\ ^2P^\circ_{3/2}$	2608.91	−7.97	−6.61	−7.80	−7.17	−6.63			−6.94	0.40
$3s3p^2\ ^4P_{5/2}$	$3s^24p\ ^2P^\circ_{3/2}$	2620.90	−4.87	−5.56	−5.00	−5.33	−4.63			−4.97	0.30
$3s3p^2\ ^2D_{3/2}$	$3s^24p\ ^2P^\circ_{1/2}$	3862.60	−0.73	−0.89	−0.50	−0.90	−0.67			−0.86	0.28
$3s3p^2\ ^2D_{3/2}$	$3s^24p\ ^2P^\circ_{3/2}$	3853.66	−1.43	−1.58	−1.20	−1.60	−1.37			−1.55	0.28
$3s3p^2\ ^2D_{5/2}$	$3s^24p\ ^2P^\circ_{3/2}$	3856.02	−0.48	−0.64	−0.25	−0.64	−0.42			−0.62	0.32
$3s^24s\ ^2S_{1/2}$	$3s^24p\ ^2P^\circ_{1/2}$	6371.36	−0.37	−0.99	−0.11	−0.21	−0.12			−0.32	0.20
$3s^24s\ ^2S_{1/2}$	$3s^24p\ ^2P^\circ_{3/2}$	6347.10	−0.55	−0.04	−0.20	−0.09	+0.19			−0.01	0.19

and $\mathcal{A}$ is an antisymmetrization operator. The functions Φ_j are bound-type functions of the total system constructed with target orbitals; they are introduced to compensate for orthogonality conditions imposed on the $F_i(r)$ and to improve short-range correlations. The Kohn variational principle gives rise to a set of coupled integro-differential equations that are solved by R-matrix techniques (Burke & Seaton 1971; Berrington et al. 1974, 1978, 1987) within a box of radius, say, $r \leq a$. In the asymptotic region ($r > a$) exchange between the outer electron and the target ion can be neglected, and the wavefunctions can be approximated by Coulomb solutions.

One-body Breit-Pauli relativistic corrections have been introduced in the R-matrix suite by Scott & Burke (1980); Scott & Taylor (1982). Inter-channel coupling is equivalent to CI in the atomic structure context.

Because of the large number of configurations and close coupling states in the representation of the target ion the scattering calculation had to be done in LS-coupling. Then, fine structure collision strengths were obtained by means of the intermediate coupling frame transformation (ICFT) method of Griffin et al. (1998).

Since we have produced a large number of target expansion to study the quality and the wavefunction it is interesting to see the effects of these various representations on the collision strengths. This comparison may be used to asses the accuracy of the collision strengths. Thus, we performed three different scattering calculations using target orbitals from models AST1, AST8, and AST9. For the first two calculations we included only
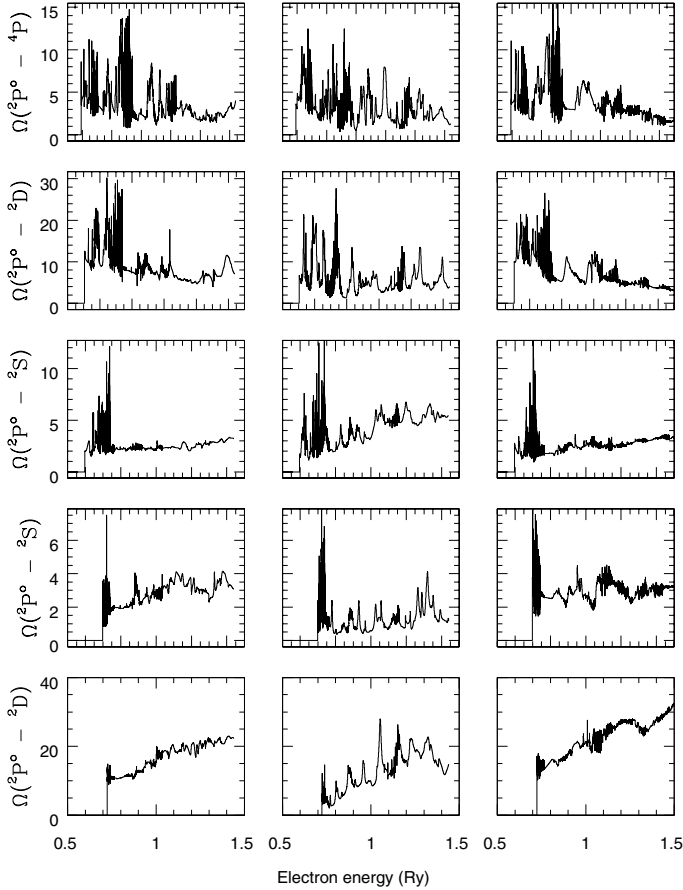
Table 4. Comparison of Maxwellian averaged collision strengths in LS-coupling for excitation from the ground term $3s^23p\ ^2P^\circ$.

Upper term	T (K)	Model 9	Difference (%)	
			model 1	model 8
$3s3p^2\ ^4P$	5000	4.44E+0	1.2	5.7
	10 000	4.36E+0	1.4	5.9
	20 000	4.43E+0	−2.4	−5.2
$3s3p^2\ ^2D$	5000	1.19E+1	−8.2	−39.8
	10 000	1.18E+1	−3.1	−36.4
	20 000	1.10E+1	3.9	−34.2
$3s^24s\ ^2S$	5000	2.17E+0	11.0	25.3
	10 000	2.18E+0	16.3	27.0
	20 000	2.21E+0	15.2	33.1
$3s3p^2\ ^2S$	5000	3.32E+0	−38.1	−52.4
	10 000	3.08E+0	−32.7	−54.7
	20 000	2.95E+0	−24.4	−59.2

the lowest 12 LS terms in the closed coupling expansion, while for the calculation with the AST9 target, the most accurate and extensive, we included the lowest 43 LS terms. All calculations explicitly include partial waves from states with $L \leq 16$ and multiplicity 1, 3, 5, and 7. The final collision strengths are produced with an energy resolution of 6×10^{-5} Ry.

Figure 4 compares the LS-coupling collision strengths obtained from the target expansions AST1, AST8, and AST9 for excitation from the ground term $3s^23p\ ^2P^\circ$ to the first four excited terms $3s3p^2\ ^4P$, $3s3p^2\ ^2D$, $3s^24s\ ^2S$, and $3s3p^2\ ^2S$.

Fig. 4. Comparison of collision strengths in LS coupling for excitations from the ground term to the first five excite terms in Si II computed with approximations AST1 (*left panels*), AST8 (*middle panels*), and AST9 (*right panels*).

Fig. 5. Collision strengths in *JJ*-coupling for transitions $3s^2 3p\ ^2P^\circ_{1/2}-3s^2 3p\ ^2P^\circ_{3/2}$ (*top panel*), $3s^2 3p\ ^2P^\circ_{3/2}-3s3p^2\ ^4P_{3/2}$ (*middle panel*), and $3s^2 3p\ ^2P^\circ_{3/2}-3s3p^2\ ^2D_{5/2}$ (*bottom panel*).

The results, in terms of Maxwellian averaged effective collision strengths, of AST1, AST8, and AST9 are also compared in Table 4 for excitations from the ground term, $3s^2 3p\ ^2P^\circ$, to the first five excited terms of Si II. Here, the third column presents the effective collision strengths from our best model AST9 and columns fourth and five present the percentage difference from these as obtained from models AST1 and AST8 respectively. These comparisons are done for temperatures between 5000 K and 20 000 K. Excitation rates for higher temperatures are of little practical interest because under these conditions the ionic fraction in Si II is too small. The are two general characteristics of collision strengths that could lead to variations in their thermal averages: (i) the background and resonances in the near threshold region, which determine the low temperature ($\Delta E/kT \leq 1$) Maxwellian averaged collision strengths and depend on the coupling of the target ion with the continuum; and (ii) the slope of the continuum towards high energies, which in dipole allowed transitions depend linearly on the oscillator strength and consequently on the quality of the target representation. It is interesting to see that the results from AST1 and AST9 agree rather well in terms of the qualitative shape of the collision strengths and the quantitative Maxwellian averaged rates, within ~10%, except for the $3s^2 3p\ ^2P^\circ-3s3p^2\ ^2S$ transition. This is in contrast to the large differences in gf-values for essentially all transitions among levels of the N-electron Si II target. The good agreement in collision strengths is because these are dominated by bound-continuum couplings of the (N+1)-electron system, which seems
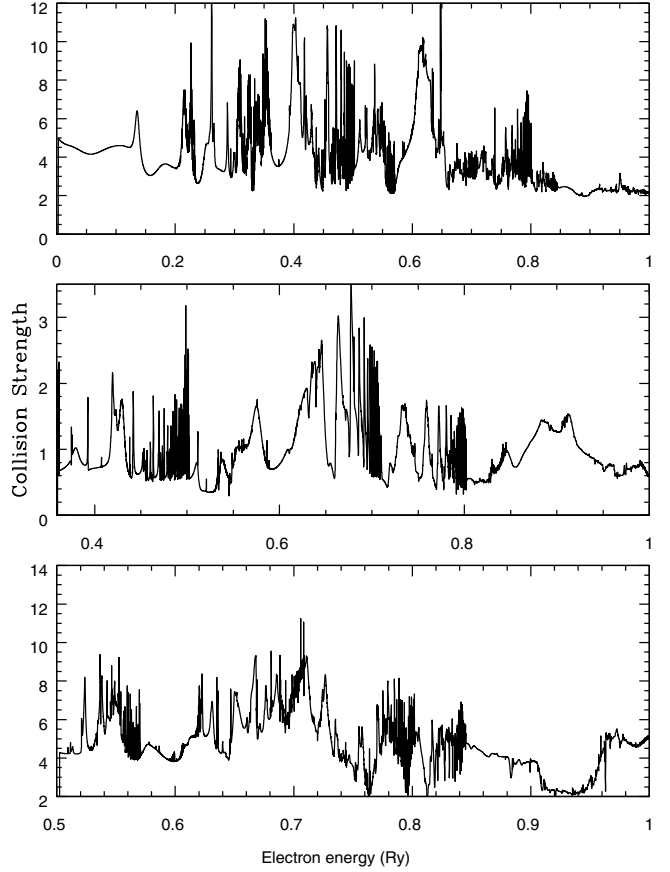
to be well represented by the large amount CI in the close coupling expansion.

On the other hand, the target expansion AST8 does yield a different lay out of resonances on the collision strengths. In addition, AST8 yields steeper rises in the background collision strengths for excitation to the $3s^2 4s\ ^2S$ level and higher levels. This translates into effective collision strengths from AST8 that are systematically lower than those from AST9 by as much as ~50%.

It is expected that our results from the AST9 expansion should be the most accurate due to the good quality of the target representation and the large amount of CI included for the ($N + 1$)-electron system. Nonetheless, the comparison with results of various target representation allow us to asses the uncertainties in the collision strengths to ~10%.

Figure 5 shows the collision strengths for a sample of forbidden, intercombination, and dipole transitions. We chose the same transitions as in Tayal (2008) for direct comparison with that work. Although the collision strengths from both calculations are roughly similar, there are quantitative differences between the two sets in terms of resonance structures and absolute level of the background. It is apparent that the present collision strengths should yield Maxwellian averages somewhat lower than those of Tayal.

In Table 5 we compare the present fine structure Maxwellian averaged collision strengths with those of Tayal (2008) and Dufton & Kingston (1991). For most transitions our results are ~30% lower than those of Tayal, while the results of

Table 5. Comparison of Maxwellian averaged collision strengths in JJ-coupling from present calculation (Present), Tayal (2008; Tayal), and Dufton & Kingston (1991; DK).

Upper level	T (K)	Present	Tayal	DK
$3s^23p$ $^2P^\circ_{3/2}$	5000	4.55	6.19	5.60
	10 000	4.45	6.09	5.70
	20 000	4.42	5.97	5.77
$3s3p^2$ $^4P_{1/2}$	5000	0.401	0.512	0.550
	10 000	0.398	0.515	0.516
	20 000	0.392	0.502	0.466
$3s3p^2$ $^4P_{3/2}$	5000	0.612	0.812	0.832
	10 000	0.609	0.789	0.780
	20 000	0.602	0.769	0.706
$3s3p^2$ $^4P_{5/2}$	5000	0.441	0.615	0.571
	10 000	0.458	0.595	0.534
	20 000	0.477	0.589	0.488
$3s3p^2$ $^2D_{1/2}$	5000	1.82	2.77	2.76
	10 000	1.82	2.74	2.74
	20 000	1.75	2.50	2.58
$3s3p^2$ $^2D_{3/2}$	5000	2.05	2.94	2.45
	10 000	2.14	2.98	2.44
	20 000	2.14	2.80	2.30
$3s^24s$ $^2S_{1/2}$	5000	0.910	1.02	1.24
	10 000	0.865	1.06	1.20
	20 000	0.857	0.979	1.04
$3s3p^2$ $^2S_{1/2}$	5000	0.887	0.102	0.716
	10 000	0.899	0.988	0.840
	20 000	0.916	0.988	0.902

variational parameters of this potential. This optimization technique takes into account the differences between length and velocity gauges of the gf-values, in addition to the accuracy of predicted energy levels. Our most accurate gf-values were then compared with previous theoretical and experimental determinations. From these comparisons we derive a recommended set of gf-values and estimate their uncertainties.

We then proceed to compute electron impact excitation collision strengths with the R-matrix method. We do so by using various of the targets representations made from the previous calculations and compare the results. This allows us to identify the physical effects that affect the accuracy of the computed collision strengths. We also compare our results with those of previous calculations. The present results agree reasonably well with those of Dufton & Kingston (1991), who also used an orthogonal R-matrix method but with a much smaller close coupling expansion. On the other hand, the present results for Maxwellian averaged collision strengths are systematically lower than those of the recent calculation of Tayal (2008) using a non-orthogonal R-matrix method. The reasons for these differences, that typically amount to ~30%, are unclear. We argue that the source of this difference could be in the non-orthogonal R-matrix approach.

Tables 6 and 7 containing the present gf-values, A-values, and effective collision strengths are available in electronic form. The data and atomic model are also to become available through the TIPTOP[1] database and the XSTAR database Bautista & Kallman (2001).

Dufton & Kingston lie inbetween those two. That our results are somewhat lower than those of Dufton & Kingston can be understood from the much larger close coupling expansion used in the present work. As more scattering channels are open in the calculation, the flow of electrons is redistributed and the collision strength among low lying levels tends to converge to lower values. The source of the differences found with respect to Tayal are less clear, and seems to be due to differences in computational approach used, i.e. between the orthogonal and non-orthogonal R-matrix methods.

4. Conclusions

We have carried out extensive calculations of transitions rates and collision strengths for electron impact excitation for the lowest 12 levels of the astrophysically important Si II ion.

In the calculation of radiative data, we paid special attention to the weak dipole allowed and intercombination transitions, which are of particular interest for plasma diagnostics. Determination of accurate data for these transitions is particularly challenging, therefore we studied the effects of valence-valence, valence-core, and core-core interactions with three different methods, i.e. MCDF, HFR, and the central potential method implemented in AUTOSTRUCTURE. With MCDF we could only include valence-valence correlations, as opening of the $n = 2$ core resulted in a large number of states that could not be managed with the computer code GRASP. For this reason, we were able to obtain accurate transition rates for the $3s^23p$ $^2P^\circ$–$3s3p^2$ ^4P intercombination transitions only. Both HFR and AUTOSTRUCTURE allowed us to investigate valence-core and core-core interaction by building very large configuration expansions. The accuracy of AUTOSTRUCTURE calculations were significantly improved by the use of the c-TFDA potential of Bautista (2008) and a new technique for optimizing the

References

Badnell, N. R. 1986, J. Phys. B, 19, 3827
Badnell, N. R. 1997, J. Phys. B, 30, 1
Baldwin, J. A., Ferland, G. J., Korista, K., et al. 1996, ApJ, 461, 664
Bautista, M. A. 2008, J. Phys. B: Atom. Mol. Opt. Phys., 41, 065701
Bautista, M. A., & Kallman, T. R. 2001, ApJS, 134, 139
Bautista, M. A., Mendoza, C., Kallman, T. R., & Palmeri, P. 2003, A&A, 403, 339
Bergeson, S. D., & Lawler, J. E. 1993, ApJ, 414, L137
Berrington, K. A., Burke, P. G., Butler, K., et al. 1987, J. Phys. B, 20, 6379
Berrington, K. A., Burke, P. G., Chang, J. J., et al. 1974, Comput. Phys. Commun., 8, 149
Berrington, K. A., Burke, P. G., Le Dourneuf, M., et al. 1978, Comput. Phys. Commun., 14, 367
Berrington, K. A., Burke, P. G., Eissner, W., et al. 1995, Comput. Phys. Commun., 92, 290
Burke, P. G., & Seaton, M. J. 1971, Meth. Comp. Phys., 10, 1
Calamai, A. G., Smith, P. L., & Bergeson, S. D. 1993, ApJ, 415, L59
Cowan, R. D. 1981, The Theory of Atomic Structure and Spectra (Berkeley, CA: University of California Press)
Curtis, L. J., & Smith, W. H. 1974, Phys. Rev. A, 9, 1537
Drake, G. W. F. 1971, Phys. Rev. A, 3, 908
Dufton, P. L., & Kingston, A. E. 1991, MNRAS, 248, 827
Dufton, P. L., Keenan, F. P., Hibbert, A., Ojha, P. C., & Stafford, R. P. 1992, ApJ, 387, 414
Dunn, J. P., Bautista, M. A., Arav, N., et al. 2009, ApJ, submitted
Dyall, K. G., Grant, I. P., Johnson, C. T., Parpia, F. A., & Plummer, E. P. 1989, Comput. Phys. Commun., 55, 425
Eissner, W., & Nussbaumer, H. 1969, J. Phys. B, 2, 1028

---

[1] http://heasarc.gsfc.nasa.gov/topbase

Eissner, W., Jones, M., & Nussbaumer, H. 1974, Comput. Phys. Commun., 8, 270

Froese Fischer, C., Tachiev, G., & Irimia, A. 2006, At. Data Nucl. Data Tables, 92, 607

García, J., Mendoza, C., Bautista, M. A., et al. 2005, ApJS, 158, 68

Griffin, D. C., Badnell, N. R., & Pindzola, M. S. 1998, J. Phys. B. At. Mol. Opt. Phys, 31, 3713

Hofmann, W. 1969, Z. Nat., 24, 990

Jenkins, E. B. 1986, ApJ, 304, 739

Johnson, W. R., Kolb, D., & Huang, K. N. 1983, At. Data Nucl. Data Tables, 28, 333

Jönsson, P., He, X., Froese Fischer, C., & Grant, I. P. 2007, Comput. Phys. Commun., 177, 597

Judge, P. G., Carpenter, K. G., & Harper, G. M. 1991, MNRAS, 253, 123

Luo, D., Pradhan, A. K., & Shull, J. M. 1988, ApJ, 335, 498

Nahar, S. N. 1988, At. Data Nucl. Data Tables, 68, 83

http://physics.nist.gov/PhysRefData/ASD/levels_form.html

Nussbaumer, H. 1977, A&A, 58, 291

Palmeri, P., Mendoza, C., Kallman, T. R., & Bautista, M. A. 2003a, A&A, 403, 1175

Palmeri, P., Mendoza, C., Kallman, T. R., Bautista, M. A., & Meléndez, M. 2003b, A&A, 410, 359

Palmeri, P., Quinet, P., Mendoza, C., et al. 2008a, ApJS, 177, 408

Palmeri, P., Quinet, P., Mendoza, C., et al. 2008b, ApJS, 179, 542

Parpia, F. A., Froese Fischer, C., & Grant, I. P. 1996, Comput. Phys. Commun., 94, 249

Quinet, P., Palmeri, P., Biémont, E., et al. 1999, MNRAS, 307, 934

Quinet, P., Palmeri, P., Biémont, E., et al. 2002, J. Alloys Comp., 344, 255

Savage, B. D., & Lawrence, G. M. 1966, ApJ, 146, 940

Schectman, R. M., Povolny, H. S., & Curtis, L. J. 1988, ApJ, 504, 921

Scott, N. S., & Burke, P. G. 1980, J. Phys. B, 13, 4299

Scott, N. S., & Taylor, K. T. 1982, Comput. Phys. Commun., 25, 349

Shull, J. M., Snow, T. P., & York, D. G. 1981, ApJ, 246, 549

Tayal, S. S. 2007, J. Phys. B: Atom. Mol. Opt. Phys., 40, 2551

Tayal, S. S. 2008, ApJS, 179, 534

Van Buren, D. 1986, ApJ, 311, 400